Electronic Supplementary Material (ESI) for Biomaterials Science.

Mechanically Robust Hybrid Hydrogels of Photo-crosslinkable Gelatin and Laminin-Mimetic Peptide Amphiphiles for Neural Induction

Melis Isik[1], Cemil Can Eylem[2], Tugba Haciefendioglu[3], Erol Yildirim[3-5], Buse Sari[1,6], Emirhan Nemutlu[2,7], Emel Emregul[1], Babatunde O. Okesola[8,9]*, Burak Derkus[1,6]*

1. Department of Chemistry, Faculty of Science, Ankara University, 06560 Ankara, Turkey
2. Analytical Chemistry Division, Faculty of Pharmacy, Hacettepe University, 06230 Ankara, Turkey
3. Chemistry Department, Middle East Technical University, Ankara 06800, Turkey
4. Department of Polymer Science and Technology, Middle East Technical University, 06800, Ankara, Turkey
5. Department of Micro and Nanotechnology, Middle East Technical University, 06800, Ankara, Turkey
6. Stem Cell Research Lab, Department of Chemistry, Faculty of Science, Ankara University, 06560 Ankara, Turkey
7. Bioanalytic and Omics Laboratory, Faculty of Pharmacy, Hacettepe University, Ankara, Turkey
8. Institute of Bioengineering, Queen Mary University of London, London, E1 4NS, UK.
9. School of Engineering and Materials Science, Queen Mary University of London, London, E1 4NS, UK.

*Corresponding authors: bderkus@ankara.edu.tr (Burak Derkus), b.okesola@qmul.ac.uk (Babatunde O. Okesola)

Supporting Information Contents

Section 6: CD analysis

Section 7: Gel characterization – SEM, Rheology, CD, Degradation

Section 8: MD simulation

Section 9: Cell behaviour – SEM and immunostaining

Section 10: Gene expression study for cellular differentiation

Section 11: Metabolomics study

Section 1: Synthesis and Characterization of GelMA: NMR and FTIR analyses

Type A porcine skin gelatin (10% w/v, Sigma-Aldrich, USA) was dissolved in Dulbecco's Phosphate Buffer Saline (DPBS) at 55°C for 1h. Methacrylic anhydride (MA, Sigma-Aldrich, USA) was pipetted at a rate of 1 ml min^{-1} to the gelatin solution under stirred conditions. After 3h of agitation, the resulting solution was diluted (4x) with DPBS to stop the reaction. The methacrylated gelatin solution was then dialyzed against distilled water through 12–14 kDa cut-off dialysis tubing for 4-5 days at 37 °C to purify the product. GelMA in powder form was obtained after a freeze-drying process.

We used ^{1}H-Nuclear Magnetic Resonance (NMR), Fourier-Transform Infrared Spectroscopy (FTIR), and UV-spectroscopy to confirm the synthesis of GelMA.

For the ^{1}H-NMR analysis, freeze-dried GelMA poweder and gelatin sample were dissolved in D2O (20 mg ml^{-1}). ^{1}H NMR spectra were obtained using a Bruker DPX 400 spectrometer (Germany) between 0-10 ppm. In addition to the characteristic peaks of gelatin backbone, the ^{1}H-NMR spectra GelMA samples showed other peaks (d = 5.3 ppm and d = 5.6 ppm), which correspond to the acrylic protons of methacrylic moiety (Figure S1).[1] In addition, the new signal at d = 1.8 ppm corresponds to the methyl group of the methacrylate moiety, thus, further confirmed methacrylation of the gelatin backbone. We determined the degree of methacrylation to be 68.65% by integrating peak area at d = 2.9 ppm as previously reported.[2] This peak corresponds to methylene moiety of the side chain lysine residue on which methacrylation occurs.

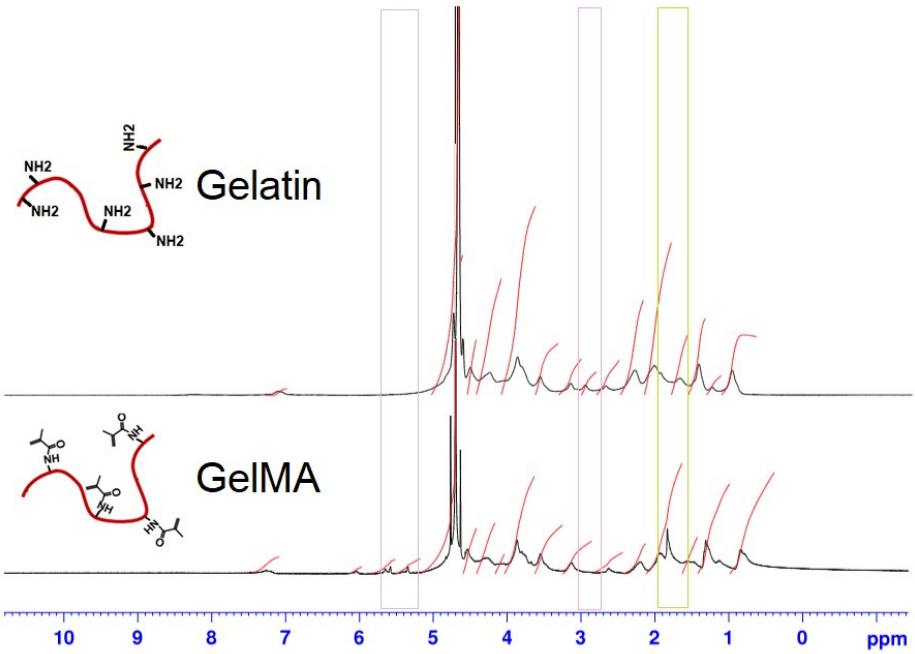

Figure S1 NMR spectra obtained with gelatin and GelMA

The synthesis of GelMA was further confirmed by FTIR (Shimadzu IRAffinity-1 (Japan). Specific peaks indicating the gelatin backbone were clearly visible at 3330 cm^{-1} (OH), 3076 cm^{-1}, (N-H stretch), 2945 cm^{-1} (saturated C-H stretch), 1680 cm^{-1} (amide I) and 1521 cm^{-1} (amide II) (Figure S2). We observed the same bands with a slight shift in the spectrum of GelMA. In addition, the spectra revealed C = C vibrational stretching at 1640 cm^{-1}. The shift at the positions of the peaks in addition to alteration in the intensity of some peaks (i.e., unsaturated C = C stress) can be considered as an indication of the modification of gelatin.[3] The increase in the amide I peak at 1629 cm^{-1} in the spectrum of GelMA is thought to be due to the amide bonds formed between amino groups and methacrylic anhydride, and this increase in the amide I band intensity supports the success of methacrylation. On the other hand, FTIR revealed that there was no change –such as denaturation, degradation, or chemical breakage– in the gelatin backbone after UV-exposure (Figure S3).

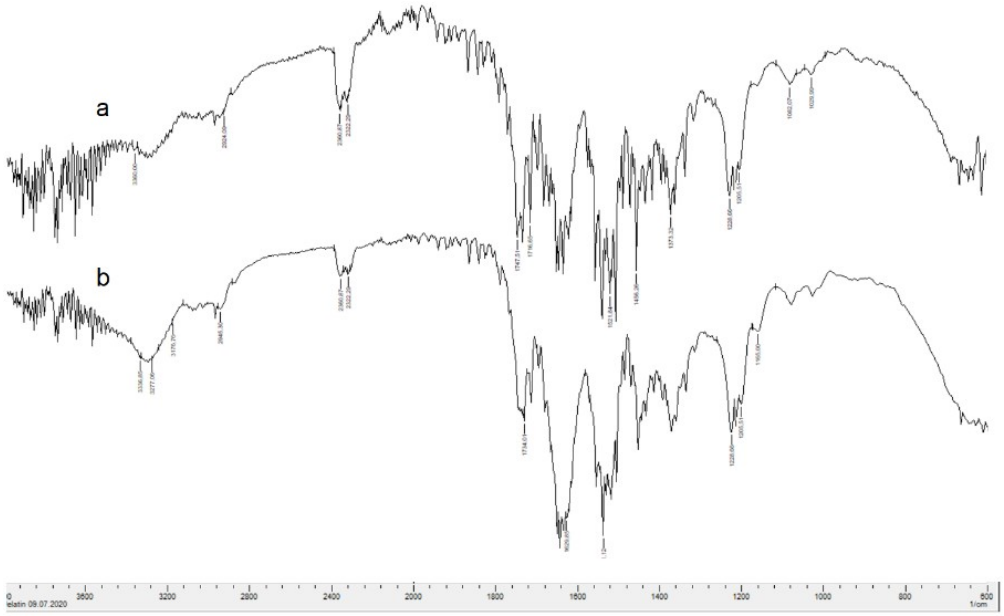

Figure S2 FTIR spectra related to gelatin (a) and GelMA (b)

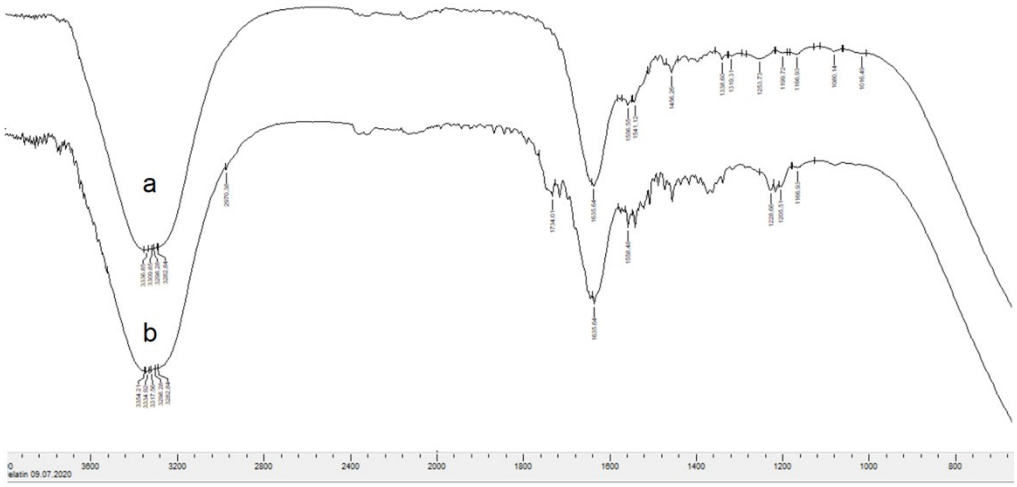

Figure S3 FTIR spectra of uncrosslinked (a) and crosslinked (b) GelMA

Transparency of GelMA was assessed by UV-spectroscopy (Thermo Scientific, USA). It was observed that GelMA (10% wt.) absorbed the light in UV-region (wavelength 200-400 nm), while it transmitted the light in the visible region (beyond 400 nm) (Figure S4). The transparency of GelMA hydrogel was also confirmed macroscopically (Figure S4).

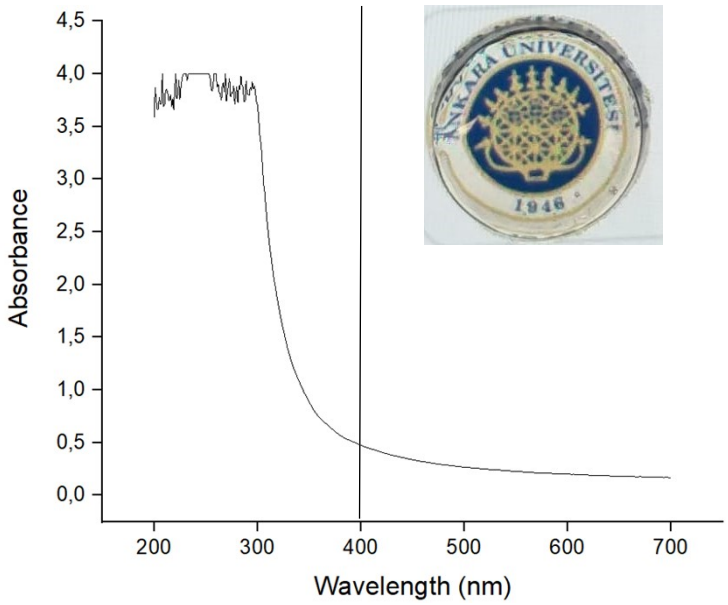

Figure S4 Optical transparancy of GelMA hydrogel

Section 2: Compression test

To identify the Young's Modulus of GelMA hydrogels in different concentrations –that were tested in cell culture applications–, compression test was applied. The hydrogels prepared in 6 mm diameter and 8 mm height were subjected to a load of 5 N at 2 mm min^{-1} loading rate (Cellscale, Canada). Young's moduli were calculated based on the stress/strain curves. All the measurements were performed in duplicate.

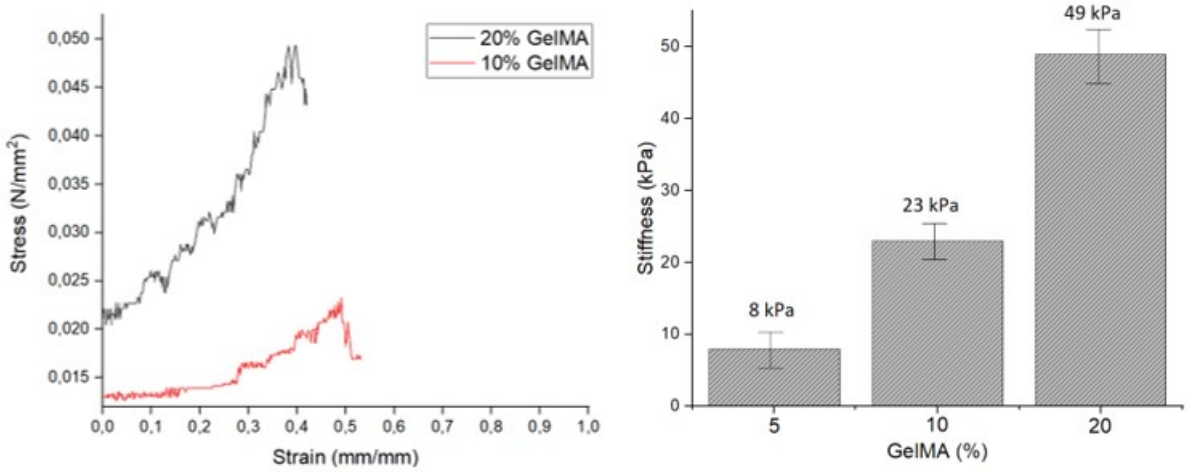

Figure S5 Compression test for 5, 10, and 20% (wt.) GelMA hydrogels

Young's modulus of GelMA hydrogels, which were tested in supramolecular hydrogel design (5, 10, and 20% GelMA), were measured with compression testing to be 8, 23, and 49 kPa, respectively (Figure S5).

Section 3: Peptide synthesis and purification

PAs (**PA-GSR(+)** and **PA-RGDS(+)**) were synthesized using solid-phase peptide synthesis method based on the 9-fluorenylmethoxycarbonyl (Fmoc) protection chemistry on an automated peptide synthesizer (Liberty Blue, CEM, USA). Rink Amide resin with 100-200 mesh (Novabiochem Corporation, USA) was used as carrier. Amino acid coupling reactions were done using 4 equivalents (4 mmol) of Fmoc-capped amino acids (Novabiochem Corporation, USA), 6 equivalents of *N,N'*-diisopropylcarbodiimide (DIC, Sigma-Aldrich, UK), and 4 equivalents of *1*-hydroxybenzotriazol (HOBT, Carbosynth, UK). Next, a hydrophobic lipid tail (palmitic acid, Alfa Aesar, USA) was conjugated to the free *N*-terminus of the synthesized peptides by using 4 equivalents of palmitic acid, 4 equivalents of HOBT, and 6 equivalents DIC in dimethylformamide (DMF) / dichloromethane (DCM) after the success of deprotection step was confirmed with Kaiser (ninhydrine) test. After an overnight proceeded alkylation reaction, the success of alkylation was tested with Kaiser test, and the PAs were cleaved from resin with a mixture of trifluoroacetic acid (TFA) / triisopropyl silane (TIS) / Water (95:2.5:2.5) for 3 h at room temperature on a shaker arm. Following a filtration step of the cleaved PAs, the TFA was evaporated and the resulting solution was precipitated with cold diethyl ether stored at -20 ^{o}C. Lastly, the precipitate was collected by centrifugation at 4000 rotations per minute (rpm), allowed to dry inside a hood overnight, and freeze-dried for 2-3 days.

For the purification of the synthesized PAs, freeze-dried crude PAs (10 mg mL^{-1}) were dissolved in TFA/Water (1% v/v). After sonication, the solutions were filtered through 0.22 μm filter and purified using Reverse Phase High Performance Liquid Chromatography-Mass Spectroscopy (RP-HPLC/MS)(Waters, USA) with a C18 column. TFA/Water and TFA/ACN were used as phases. Finally, the purified PAs were freeze-dried for 2-3 days to obtain a fluffy white product, and kept in -20 ^{o}C until use.

PA-GSR(-) was obtained commercially.

Section 4: Characterization of PAs – TEM

The morphologies of the PAs were investigated using TEM. In this context, PAs were counterstained on TEM grids. 10 μL of sample injected onto a piece of parafilm and the TEM

grid was laid down onto droplet, and allowed to adsorb PAs for 10 s. After removing the excess liquid, same operation was repeated with water three times to remove the excess and unbounded PAs. Finally, the PAs were stained with uranyl acetate on droplets. The images were acquired with a JEOL 1230 TEM at 80 kV energy.

Section 5: Zeta potential measurement

Zeta potentials (ζ) were measured to determine the overall charges of **PA-GSR(+)**, **PA-GSR(-)**, and **PA-RGDS(+)** and **GelMA** on a Zetasizer (MPT-2 Instrument, Malvern Panalytical, UK). PAs were dissolved (0.1% wt.) in HEPES(4-(2-hydroxyethyl)-1-piperazineethanesulfonic acid) buffer, pH was adjusted to 7.4, and measurements were conducted. Each measurement was repeated three times.

Section 6: CD analyses

To identify the conformation of the synthesized and purchased PAs, CD analyses were conducted using a spectropolarimeter instrument (JASCO J81, Japan). Aqueous solutions of PA molecules (0.1 wt.) were loaded into quartz cuvettes with 1 cm path length and spectra were acquired. Measurements were performed within the range of 180–260 nm.

Section 7: Gel characterization – SEM, Rheology, CD, Degradation

Hydrogel microstructures were characterized using SEM. Gels were processed for SEM with freeze-dryer to remove the water and other solvents. The gels were washed, frost overnight, freeze-dried for 1d, sputter-coated with gold at 20 mA for 45 s, and monitored under SEM (FEI 430 Nova NanoSEM, USA). The mechanical properties of **PA-GSR(+)** hydrogel, **GelMA(-)/PA-GSR(+)** before and after UV-exposure were examined with oscillatory rheology (TA Instruments, Waters, USA). Frequency sweep mode was used to obtain spectra. To observe the conformational change in the co-assembled supramolecular hydrogel, CD spectra were obtained for **GelMA(-)/PA-GSR(+)** by mixing **GelMA(-)** (1 mg ml^{-1}) either with **PA-GSR(+)** (1 mg ml^{-1}) or **PA-GSR(-)** (1 mg ml^{-1}) (1:1 v/v). Measurements were conducted as described in Section 6. Biodegradation test was performed by weighting hydrogel samples (GelMA/PA-GSR(+), n=3) before and after degradation times (1, 3, 7, and 10 days). The gels before weighting were freeze-dried and the degradation percent was calculated using the equation below:

$$\% \text{ Degradation} = [(W_{initial} - W_{final}) / W_{initial}] \times 100$$

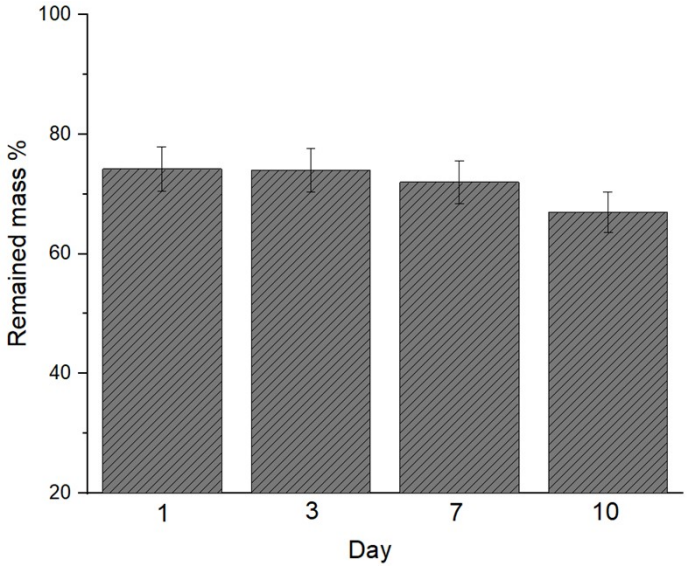

Figure S6 Degradation kinetics for **GelMA(-)/PA-GSR(+)** hydrogels

Section 8: MD simulation

A more comprehensive and realistic MD simulation on the GelMA surface and peptide interface in water under periodic boundary conditions were further performed. 4 units of GelMA were used to form a linear chain and 4 linear chains were used to form a planar two-dimensional hydrogel. The three-dimensional structure of GelMA hydrogel was constructed by crosslinking 4-layers of these planar chains, which ultimately led to the formation of 64 units that were randomly bonded to each other. Next, GelMA hydrogel was placed into an empty unit cell with a density as low as 0.2 g cc^{-1}, followed by initial model energy minimization with cell optimization to obtain a stable configuration. The optimized cell was enlarged 20 Å in the z-direction to form a vacuum over the surface, and 1968 water molecules were packed into the gel and vacuum resulting in a final density of 1.14 g cc^{-1} with the cell parameters 6 nm x 6 nm x 5 nm. Energy minimization was performed for swollen hydrogel with a water interface. Finally, **PA-GSR(+)** and **PA-GSR(-)** were added to the three different locations on the surface to perform the molecular simulation under the canonical (NVT) ensemble with a time step of 1 fs for 2 ns total simulation time until the system reached equilibrium. The trajectory of the system was saved for every 5000 steps, thermostat was selected as Nose, and simulation temperature was set to 300 K. Last 10 frames were analyzed for the average total, electrostatic and vdW energy of the system for the GelMA hydrogel with water having a peptide on the surface.

Pairwise mixing energy between **GelMA(-)** and **PA-GSR(+)** or **PA-GSR(-)**) without solvent or surface effect is presented in Table S1.

Table S1. Mixing energies based on the cohesive energy densities.

	Pairwise mixing	**MD simulation on surface**			
kcal/mol	ΔE_{mix}	$E_{interaction}$ (Total)	$E_{interaction}$ (Electrostatic)	$E_{interaction}$ (vdW)	R_g (Å)
GelMA/PA-GSR(+)	-421.77	-557.13	-451.80	-105.33	10.31
GelMA/PA-GSR(-)	-217.28	-430.26	-346.78	-83.48	8.48

Section 9: Cell behaviour – SEM and immunostaining

To visualize the cell adhesion, sprading, and infiltration, SEM and immunofluorescence studies were conducted. For SEM, the cells after 3-days of culture period were chemically fixed using glutaraldehyde (4% v/v) and formalin (10% v/v) in PBS solution for 20 min. After a washing step, the cells were dehydrated in a graded alcohol series (30%, 50%, 70%, 80%, 90%, and 100% ethanol), 5 min in each concentration. Finally, the constructs were freeze-dried and coated with gold before SEM imaging. For immunostaining, the cells were fixed with paraformaldehyde (4% v/v), permeabilized with Triton-X100 (0.1% v/v), treated with BSA (1% w/v) for preventing non-specific binding, incubated with β-actin primary antibody (1:100, Santa Cruz, USA), incubated with secondary antibody goat anti-mouse IgG (1:1000, Thermo Scientific, USA), incubated with DAPI (Thermo Scientific), and observed under a fluorescent microscope at 488 nm excitation (Leica DMIL, Germany).

Section 10: Gene expression study for cellular differentiation

At the end of a 10-days culture, total RNA was extracted from gels using a total RNA isolation kit (GeneDireX, USA), quantified with a spectrophotometer (Thermo Scientific, Multiskan Sky Microplate Spectrophotometer), and a total of 120 ng RNA was reverse-transcribed using iScript cDNA Synthesis Kit (Bio-Rad, USA). For real-time qPCR, each reaction was run (Bio-Rad CFX96 instrument) in duplicate on a 96-well plate using SYBR green mastermix, and the gene expressions were normalized to GAPDH. The difference or similarity in groups were evaluated by ANOVA Post Hoc Tukey test. The primer sequences used were as below:

GAPDH (housekeeping):
F CGTGGAAGGACTCATGACCA

R CAGTCTTCTGGGTGGCAGTGA

CD90
F ATGAACCTGGCCATCAGCA
R GTGTGCTCAGGCACCCC
CD105
F CCACTAGCCAGGTCTCGAAG
R GATGCAGGAAGACACTGCTG

Nestin
F CTCAGCACCGCTAACAGAGG
R CATTGGCGCTTCGGACAAG

SOX2
F ATGCACCGCTACGACGTGA
R CTTTTGCACCCCTCCCATTT

MAP2
F CAGCGTTGGAACAGAGGTTGG
R TGGCACAGGTGTCTCAAGGGTAG

Tuj1
F GGCCTTTGGACATCTCTTC
R CTCCGTGTAGTGACCCTTG

GFAP
F GTACCAGGACCTGCTCAAT
R CAACTATCCTGCTTCTGCTC

Section 11: Metabolomics study

Metabolomics analyses were performed using gas chromatography-mass spectrometry (GC-MS) and liquid chromatography quadrupole time-of-flight mass spectrometry (LC–qTOF-MS). Briefly, cell seeded hydrogels were taken out from incubator and metabolites extracted methanol: water mixture (9:1, v/v, 1 mL). The samples were transferred into Eppendorf tubes and vortexed and centrifuged at 10000 rpm for 10 min. Two aliquots containing 200 µL supernatant from each sample were completely dried in vacuum concentrator. Finally, the samples were analyzed by GC-MS and LC-qTOF-MS.

GC-MS based metabolomic analyses: The dried samples were methoxylated using methoxyamine hydrochloride in pyridine (20 mg mL^{-1}) for 90 min at 30°C. Shortly after, the samples were derivatized using *N*-methyl-*N*-trimethylsilyl trifluoroacetamide (MSTFA) and trimethylchlorosilane (TMCS, 1%) for 30 min at 37°C. Samples transferred to silylated vials were analyzed by GC-MS system (GC-MS-QP-2010 Ultra system, Shimadzu, Japan) with a

DB5-MS column (30 m +10 m duraguard × 0.25 mm i.d. and 0.25-µm film thickness). The run duration and injection volume were set at 37.5 min 1 µL, respectively. The MS scan data were collected in the range of 50–650 m/z using GC-MS Solution (Shimadzu, ver. 4.20). Injection temperature and flow rate was set at 290°C and 0.99 mL min^{-1}, respectively. Solvent delay time was adjusted to 5.90 min.

LC-qTOF-MS based metabolomic analyses: The dried samples were diluted with water (containing 0.1% FA) and acetonitrile (containimg 0.1% FA) mixture (1:1, v/v). Then, the samples were transferred to vials and analyzed using LC–qTOF-MS system (Agilent 6530 accurate-mass, Santa Clara, USA) operated with an electrospray ion source (ESI) in positive and negative ionization mode. Chromatographic separation was performed using C18 column (2.1 x 100 mm, 2.7 µm) with a mobile phase of 0.1% FA containing water (A) and 0.1% FA containing acetonitrile (B) with gradient elution (0–1 min, 10% B, 1–14 min 10−90% B, 14–15 90% B, 15–20 min 90–10%, 20–25 90-10% B). The flow rate was set at 0.3 mL min^{-1} and injection volume was 20 µL. Capillary voltage and gas temperature was adjusted to 3500 V and 300 °C, respectively. The MS scan data were acquired in the range of 100–1700 m/z using Mass Hunter Data Acquisition B.08.00 (Agilent, USA). The QC samples were analyzed in targeted MS\MS mode at 10, 20 and 40 eV for a reliable identification.

Metabolomics data analysis: Deconvolution, peak alignment and metabolite identification were carried out with MS-DIAL (ver. 4.48) software for the both metabolomic data. Peak annotations were done in GC-MS using retention index libraries. For LC-qTOF-MS based metabolomic analysis, formula predictions, and structure elucidations by means of unknown spectra were done by querying the acquired MS/MS data against the Human Metabolome Database (HMDB), Lipid Maps, Chemical Entities of Biological Interest (ChEBI) and PubChem with MS-Finder (ver. 3.50) software. TIC normalization was done for raw data set and mean scaling was applied to identified metabolite list in each group. Statistical analysis was carried out in Metaboanalyst 5.0 and 50% of the values missing were excluded from the data matrix, and PLS-DA, heatmap, one-way ANOVA, volcano, pathway impact plots were created.

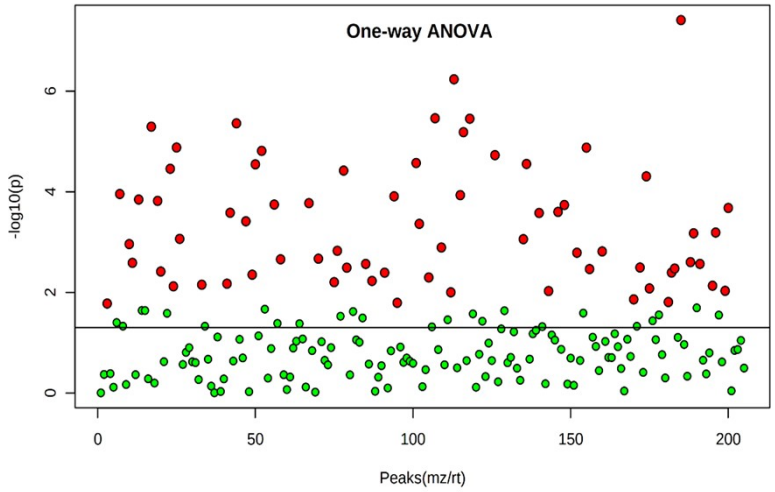

Figure S7 One-way ANOVA test applied in hMSCs that were cultured within **GelMA(-)** (GM), **GelMA(-)/PA-GSR(+)** (GM), **GelMA(-)/PA-GSR(+)** (N2B27)**, GelMA(-)/PA-RGDS(+)** (GM).

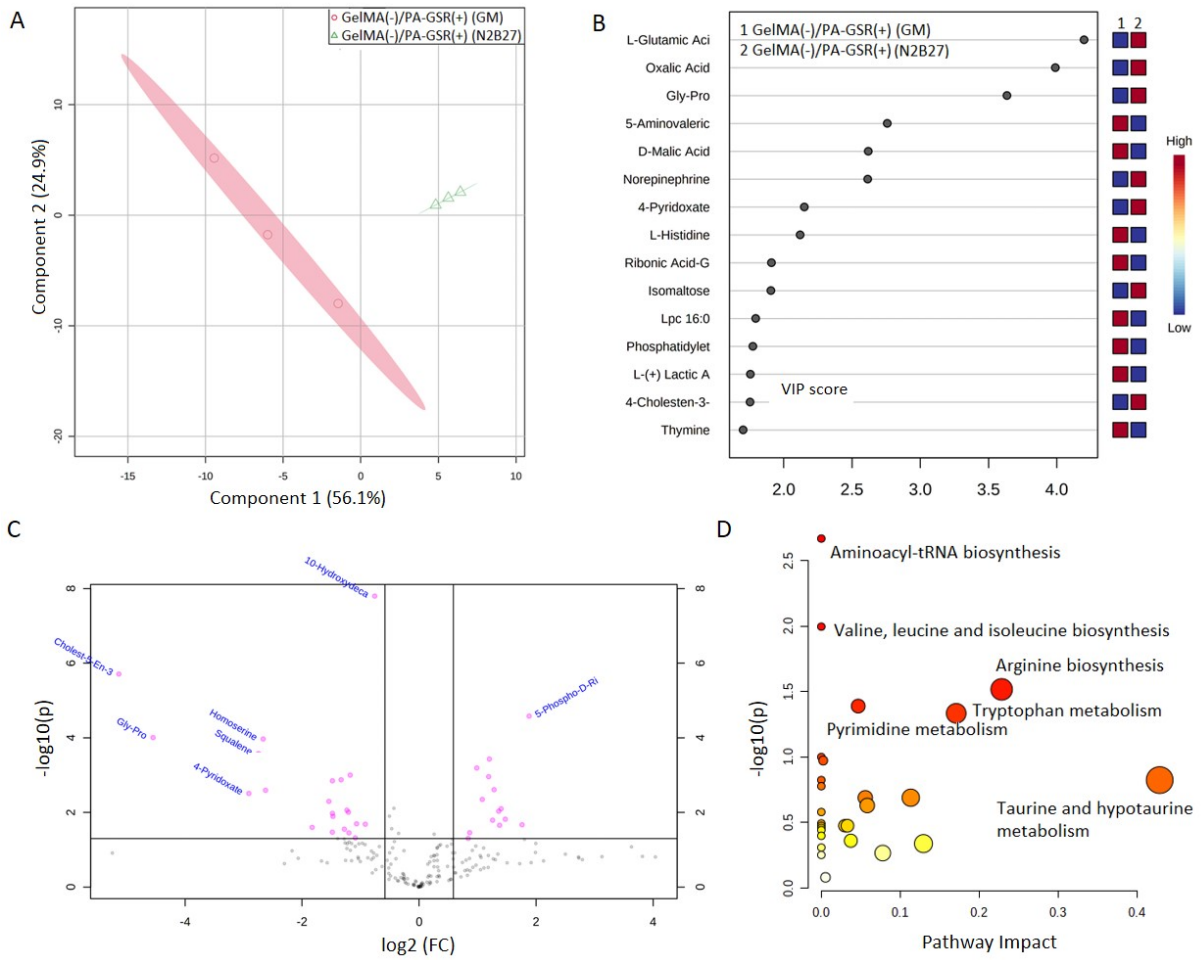

Figure S8. PLS-DA score plot that represents the discrimination of metabolite profile of hMSCs that were cultured within **GelMA(-)/PA-GSR(+)** in GM or N2B27 (n=3) (A). VIP score plot indicating the top 15 most significantly altered metabolites between the groups (n=3) (B). Volcano graph comparing differentially expressed metabolites and representing the distribution (n=3) (C). Pathway impact graph representing the affected pathways (D).

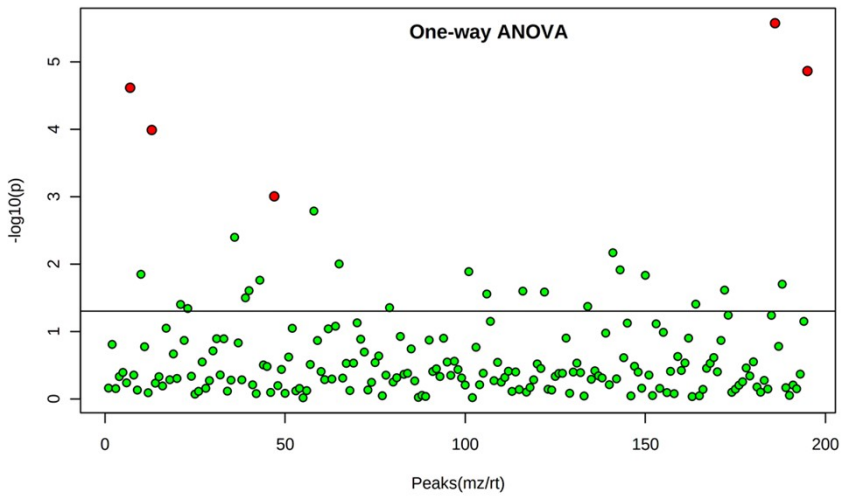

Figure S9 One-way ANOVA test applied for SH-SY5Y culture within **GelMA(-)** (N2B27), **GelMA(-)/PA-GSR(+)** (RA+BDNF), **GelMA(-)/PA-GSR(+)** (GM), **GelMA(-)/PA-RGDS(+)** (GM).

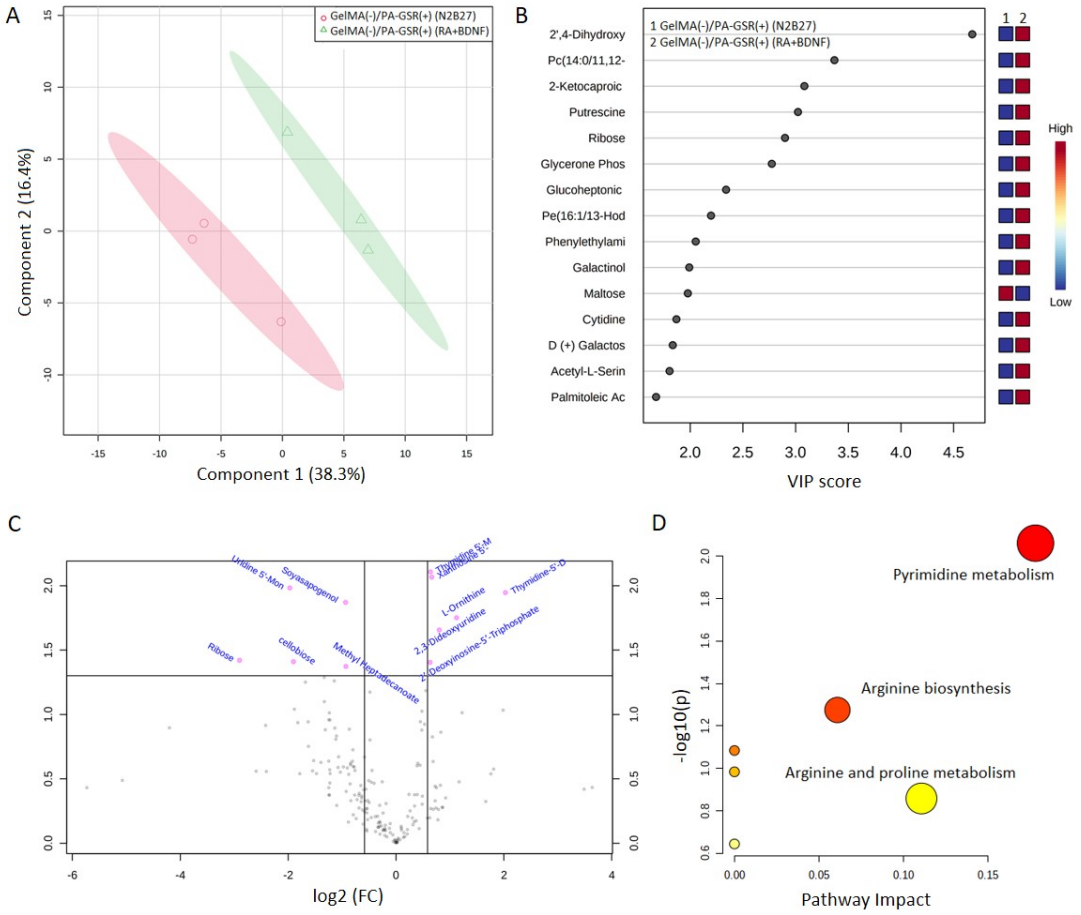

Figure S10. PLS-DA score plot that represents the discrimination of metabolite profile in SH-SY5Y cells that were cultured within **GelMA(-)/PA-GSR(+)** in N2B27 or RA+BDNF (n=3) (A). VIP score plot indicating the top 15 most significantly altered metabolites in SH-SY5Y cells that were cultured within **GelMA(-)/PA-GSR(+)** in N2B27 or RA+BDNF (n=3) (B). Volcano graph representing the distribution of altered metabolites and comparing differentially

expressed metabolites in SH-SY5Y cells (n=3) (C). Pathway impact graph representing the affected pathways in SH-SY5Y cells after neuronal induction (D).

Table S2 Affected pathways in hMSCs comprising the four groups (MetaboAnalyst 5.0)

Pathway Name	Match Status	p-value	-log(p)
Valine, leucine and isoleucine biosynthesis	4/8	5.6344E-5	4.2492
Aminoacyl-tRNA biosynthesis	7/48	5.5778E-4	3.2535
Arginine biosynthesis	4/14	6.9981E-4	3.155
Citrate cycle (TCA cycle)	3/20	0.023185	1.6348
Pyrimidine metabolism	4/39	0.032135	1.493
Alanine, aspartate and glutamate metabolism	3/28	0.05586	1.2529
Glyoxylate and dicarboxylate metabolism	3/32	0.077494	1.1107
Butanoate metabolism	2/15	0.079123	1.1017
Glycine, serine and threonine metabolism	3/33	0.083407	1.0788
Arginine and proline metabolism	3/38	0.11571	0.93664
Pantothenate and CoA biosynthesis	2/19	0.11905	0.92426
Tryptophan metabolism	3/41	0.13705	0.86311
Propanoate metabolism	2/23	0.16286	0.78817
Primary bile acid biosynthesis	3/46	0.17533	0.75613
Nitrogen metabolism	1/6	0.17556	0.75556
D-Glutamine and D-glutamate metabolism	1/6	0.17556	0.75556
Glutathione metabolism	2/28	0.22087	0.65586
Taurine and hypotaurine metabolism	1/8	0.22708	0.64382
Vitamin B6 metabolism	1/9	0.25164	0.59922
Phenylalanine metabolism	1/10	0.27544	0.55998
Cysteine and methionine metabolism	2/33	0.2804	0.55222
Valine, leucine and isoleucine degradation	2/40	0.36316	0.43991
Nicotinate and nicotinamide metabolism	1/15	0.38373	0.41597
Tyrosine metabolism	2/42	0.38627	0.41311
Histidine metabolism	1/16	0.40341	0.39426
Fatty acid biosynthesis	2/47	0.44243	0.35416
Fructose and mannose metabolism	1/20	0.47613	0.32228
beta-Alanine metabolism	1/21	0.4929	0.30724

Pathway Name	Match Status	p-value	-log(p)
Aminoacyl-tRNA biosynthesis	5/48	0.0021365	2.6703
Valine, leucine and isoleucine biosynthesis	2/8	0.01006	1.9974
Arginine biosynthesis	2/14	0.030342	1.5179
Pyrimidine metabolism	3/39	0.040706	1.3903
Tryptophan metabolism	3/41	0.046223	1.3351
Galactose metabolism	2/27	0.099736	1.0011
Alanine, aspartate and glutamate metabolism	2/28	0.10611	0.97426
Ascorbate and aldarate metabolism	1/8	0.14955	0.82521
Taurine and hypotaurine metabolism	1/8	0.14955	0.82521
Vitamin B6 metabolism	1/9	0.16665	0.7782
Steroid biosynthesis	2/42	0.20411	0.69013
Tyrosine metabolism	2/42	0.20411	0.69013
Primary bile acid biosynthesis	2/46	0.23394	0.63089
Nicotinate and nicotinamide metabolism	1/15	0.26246	0.58094
Pantothenate and CoA biosynthesis	1/19	0.32031	0.49443
Selenocompound metabolism	1/20	0.33407	0.47616
Citrate cycle (TCA cycle)	1/20	0.33407	0.47616
Fructose and mannose metabolism	1/20	0.33407	0.47616
beta-Alanine metabolism	1/21	0.34757	0.45896
Pyruvate metabolism	1/22	0.36079	0.44274

Table S3 Affected pathways in hMSCs that were cultured within **GelMA(-)/PA-GSR(+)** in GM or N2B27 (MetaboAnalyst 5.0)

Table S4 Affected pathways in SH-SY5Y cells comprising the four groups (MetaboAnalyst 5.0)

Pathway Name	Match Status	p-value	-log(p)
Arginine biosynthesis	2/14	0.0074414	2.1283
Pentose phosphate pathway	2/22	0.018063	1.7432
Phenylalanine, tyrosine and tryptophan biosynthesis	1/4	0.038188	1.4181
Arginine and proline metabolism	2/38	0.050279	1.2986
Pyrimidine metabolism	2/39	0.052703	1.2782
Aminoacyl-tRNA biosynthesis	2/48	0.076316	1.1174
Ubiquinone and other terpenoid-quinone biosynthesis	1/9	0.084009	1.0757
Phenylalanine metabolism	1/10	0.092925	1.0319
Glycerolipid metabolism	1/16	0.14474	0.8394
beta-Alanine metabolism	1/21	0.1858	0.73095
Lysine degradation	1/25	0.21732	0.66291
Glutathione metabolism	1/28	0.2402	0.61943
Glyoxylate and dicarboxylate metabolism	1/32	0.26974	0.56905
Glycine, serine and threonine metabolism	1/33	0.27696	0.55759
Biosynthesis of unsaturated fatty acids	1/36	0.29821	0.52548
Arachidonic acid metabolism	1/36	0.29821	0.52548
Amino sugar and nucleotide sugar metabolism	1/37	0.30516	0.51547
Tyrosine metabolism	1/42	0.33897	0.46984
Purine metabolism	1/65	0.47565	0.32272

Table S5. Affected pathways in SH-SY5Y that were cultured within **GelMA(-)/PA-GSR(+)** in N2B27 or RA+BDNF (MetaboAnalyst 5.0)

Pathway Name	Match Status	p-value	-log(p)
Pyrimidine metabolism	2/39	0.008684	2.0613
Arginine biosynthesis	1/14	0.053068	1.2752
Pentose phosphate pathway	1/22	0.082324	1.0845
Glutathione metabolism	1/28	0.10377	0.98393
Arginine and proline metabolism	1/38	0.13858	0.8583
Purine metabolism	1/65	0.22699	0.64399

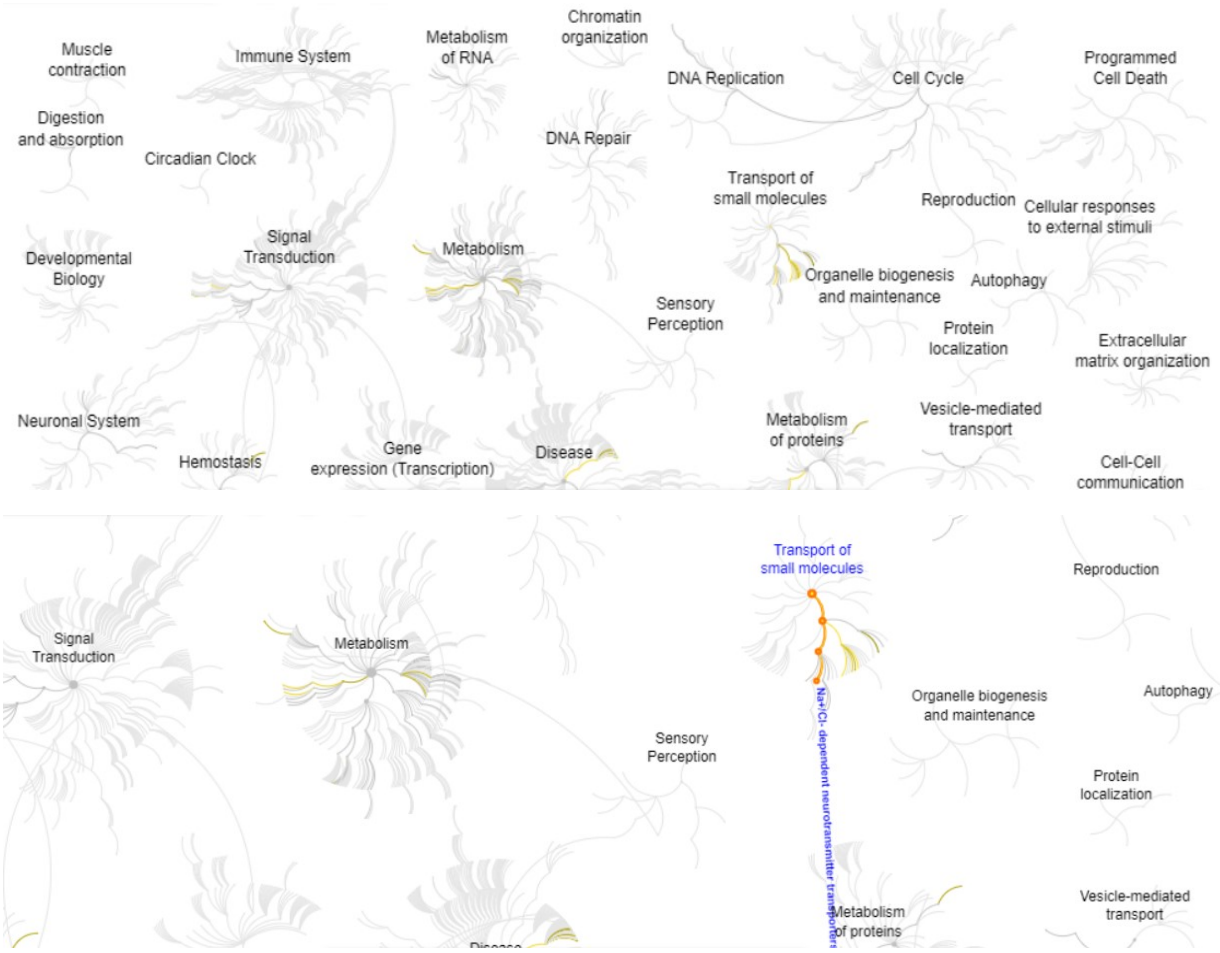

Figure S11 Interactome diagram representing the affected cellular processes and pathways as a result of inudction of hMSCs in **GelMA(-)/PA-GSR(+)** (N2B27 vs GM) (reactome.org)

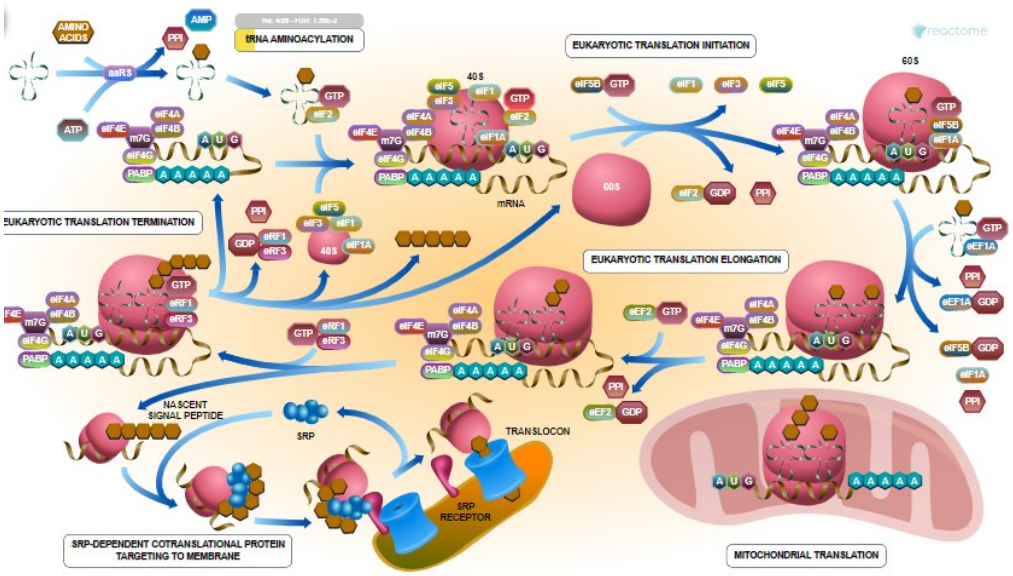

Figure S12 Significantly altered metabolites affect metabolism of proteins and translation processes by tRNA aminoacylation in hMSCs in **GelMA(-)/PA-GSR(+)** (N2B27 vs GM) (reactome.org)

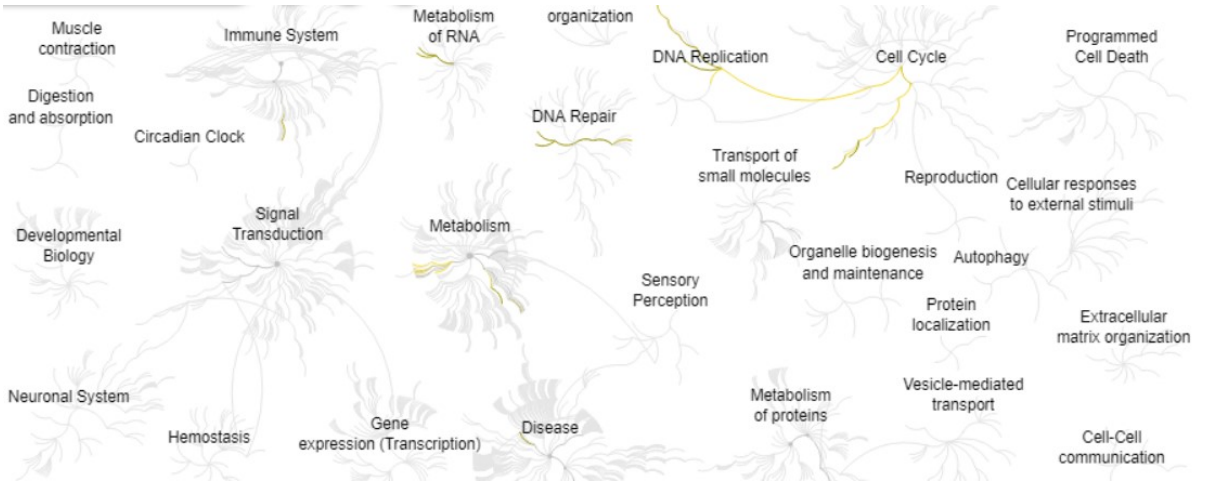

Figure S13 Interactome diagram representing the affected cellular processes and pathways as a result of inudction of SH-SY5Y cells in **GelMA(-)/PA-GSR(+)** (RA+BDNF vs N2B27) (reactome.org)

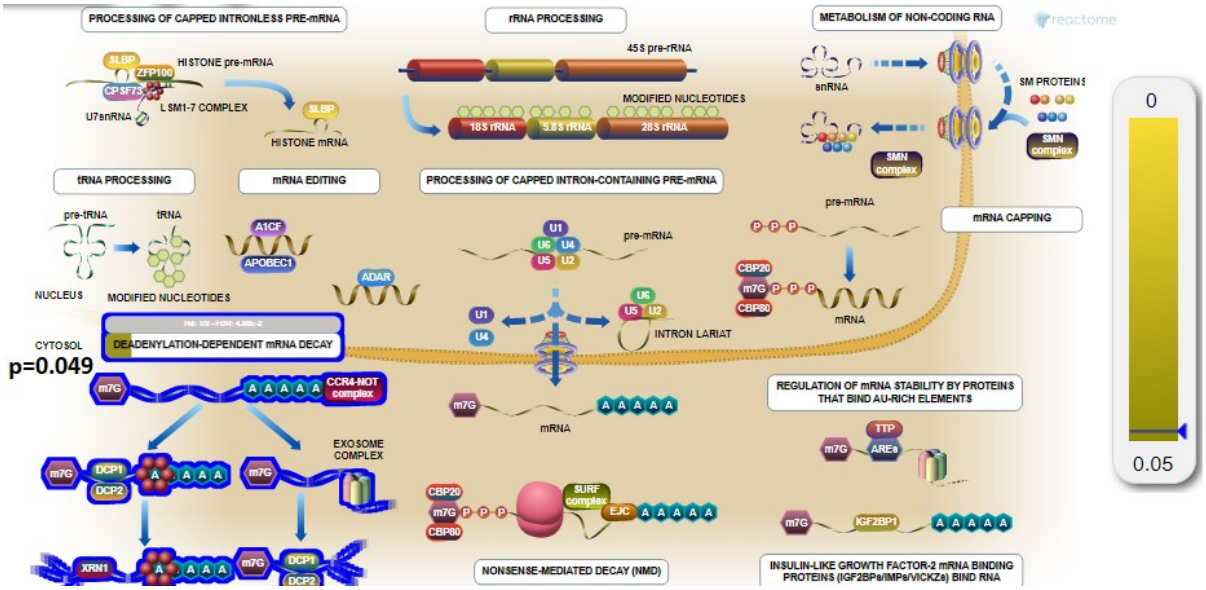

Figure S14 Significantly altered metabolites affect nucleotide metabolism, deadenylation-dependent mRNA decay, and ultimately protein metabolism in SH-SY5Y cells (RA+BDNF vs N2B27) (reactome.org).

References

(1) M. Zhu, Y. Wang, G. Ferracci, J. Zheng, N-J. Cho, and B. H. Lee. *Sci Rep*. **2019**, *9*, 6863.

(2) E. Hoch, C. Schuh, T. Hirth, G. E. M. Tovar, K. Borchers. *J Mater Sci: Mater Med,* **2012**, *23*, 2607–2617

(3) K. Modaresifar, A. Hadjizadeh, H. Niknejad, *Artif Cells Nanomed Biotechnol.*, **2017**, *46(8)*, 1799-1808.